Archives of Biochemistry and Biophysics
Vol. 373, No. 1, January 1, pp. 261–270, 2000
Article ID abbi.1999.1522, available online at http://www.idealibrary.com on IDEAL®

Serum Albumin–Lipid Membrane Interaction Influencing the Uptake of Porphyrins

Rita Galántai,* Irén Bárdos-Nagy,* Károly Módos,* József Kardos,† Péter Závodszky,‡ and Judit Fidy*,[1]

*Institute of Biophysics and Radiation Biology, Semmelweis University of Medicine, H-1444 P.O.B. 263, Budapest, Hungary; †Department of Biochemistry, Eötvös University, H-1088 Puskin u. 3, Budapest, Hungary; and ‡Institute of Enzymology, Biological Research Center, Hungarian Academy of Sciences, H-1113 Karolina út 29, Budapest, Hungary

Received July 29, 1999, and in revised form September 21, 1999

It is frequently observed in pharmaceutical practice that entrapped substances are lost rapidly when liposomes are used as carriers to introduce substances into cells. The reason for the loss is the interaction of serum components with liposomes. To elucidate the mechanism of this phenomenon the partition of mesoporphyrin (MP) was systematically studied in model systems composed of various lipids and human serum albumin (HSA). As surface charge is an important factor in the interaction, neutral (1,2-dimyristoyl-*sn*-glycero-3-phosphatidylcoline, DMPC) and negatively charged (1,2-dimyristoyl-*sn*-glycero-3-phosphatidylcoline/1,2-dimyristoyl-*sn*-glycero-3-phosphatidylglycerol, DMPC/DMPG = 19/1 w/w) lipids were compared. The liposome/apomyoglobin system was the negative control. The size distribution of sonicated samples was carefully analyzed by dynamic light scattering. Constants of association of MP to the proteins and to the liposomes were determined: $K_{p,1} = (2.5 \pm 0.7) \times 10^7\ M^{-1}$, $K_{p,2} = (1.0 \pm 0.7) \times 10^8\ M^{-1}$, $K_{L,1} = (1.3 \pm 0.3) \times 10^5\ M^{-1}$, and $K_{L,2} = (3.2 \pm 0.6) \times 10^4\ M^{-1}$ for HSA, apomyoglobin, DMPC, and DMPC/DMPG liposomes, respectively. These data were used to evaluate the partition experiments. The transfer of MP from the liposomes to the proteins was followed by fluorescence spectroscopy. In the case of apomyoglobin, the experimental points could be interpreted by ruling out the protein–liposome interaction. In the case of HSA, the efflux of MP from the liposomes was strongly inhibited above a critical HSA concentration range for negatively charged vesicles. This effect was interpreted as the result of HSA coat formation on the liposome surface. This direct interaction is significant for small liposomes. The interpretation is fully supported by differential scanning calorimetry experiments.

Key Words: **human serum albumin; mesoporphyrin; liposome; differential scanning calorimetry; fluorescence.**

In living organisms porphyrins, as prosthetic groups of enzymes and carrier proteins, are essential for several functions such as electron transport in oxidation–reduction processes of cells, oxygen transport, and storage. Thus, extensive studies have been carried out with respect to their endogenous synthesis, transport, and degradation (1–4). The observation that a class of photochemically active dyes including porphyrins selectively accumulates in tumorous cells has attracted special interest in porphyrin derivatives as candidates for therapeutic and diagnostic applications (5–7). In some applications, the targeted delivery of phorphyrins (or other effector molecules) is achieved by incorporation into liposomes (8, 9). Evidence has shown that the metabolism and transport of porphyrins involve, at certain points, the crossing of biological (or artificial) membranes (10, 11). Plasma components, however, may significantly influence these processes including the general application of liposomes as carriers or the lysis of lipid vesicles, as numerous data show (12–15).

In the present work, liposomes as carriers in targeted delivery and as models of biological membranes were studied in the presence of human serum albumin (HSA).[2] It is well known that HSA effectively binds the

[1] To whom correspondence should be addressed. Fax: 36–1–266–6656. E-mail: judit@puskin.sote.hu.

[2] Abbreviations used: HSA, human serum albumin; BSA, bovine serum albumin; MP, mesoporphyrin IX; DMPC, 1,2-dimyristoyl-*sn*-glycero-3-phosphatidylcoline; DMPG, 1,2-dimyristoyl-*sn*-glycero-3-

0003-9861/00 $35.00

porphyrin derivatives (2, 16), but the details of porphyrin transfer from the lipid phase of the liposome or the membrane to the protein are not fully known. We focused our attention on the question of whether direct interaction occurs between the protein and the membrane. This question is related to the nonspecific paracellular transfer mechanism of albumin (17). There are contradictions concerning the binding of albumin to artificial membranes among the results of different studies. Evidence has been published for the binding of albumin to liposomes and it was found to be independent of surface charge (18). Other data for the distribution of deuteroporhyrin between DMPC liposomes and serum albumin have been interpreted without supposing an interaction between the protein and the membrane (19). In other works, the results seemed to provide evidence for liposome–albumin interaction, but the authors did not consider this interpretation of the data (4). The lack of a final conclusion regarding liposome–albumin interaction is certainly connected to the fact that experimental conditions (lipid composition, method of preparation of liposomes, pH, temperature, [albumin]/[lipid] molar ratio, homogeneity and source of albumin, etc.) have an important effect, and thus it is hard to find fully comparable data in the literature.

In our previous studies, we revealed a difference in the transfer of free base– and Mg–mesoporphyrin from liposomes to HSA. The data were interpreted as the result of protein–liposome interaction (20).

In the present work, we report results of a systematic study with the goal of obtaining experimental evidence concerning a direct interaction between human serum albumin and liposomes of neutral (DMPC) and negatively charged (DMPC/DMPG, 19/1 w/w) surfaces. We show that such an interaction may influence mesoporphyrin IX (MP) transport from the lipid membrane to HSA. MP was selected for the experiments because of its photostability and relatively high solubility in organic and aqueous solutions (21), which are very important factors in the correct evaluation of the data. MP is a porphyrin derivative that is naturally metabolized only by bacteria (22). Its chemical structure does not differ too much from the free base porphyrin derivatives, more common in human metabolism and therapeutic applications; therefore, the generalization of the results is obvious. The negative surface charge of liposomes was achieved by adding DMPG, because it is a natural component of the mitochondrial membrane. The mitochondria are the location of porphyrin synthesis, and proved to be the binding site of photosensitizers in cells (23–25). Due to the negative charge and hydroxyl groups of the phosphatidylglycerol headgroups, these lipids are most probably involved in the interaction of membranes with ions and proteins (26, 27).

phosphatidylglycerol; DMF, dimethylformamide; ApoMb, apomyoglobin; SUV, small unilamellar vesicle; LUV, large unilamellar vesicle; DSC, differential scanning calorimetry; MEM, maximum entropy method.

MATERIALS AND METHODS

Chemicals. The samples were prepared in 10 mM sodium phosphate buffer at pH 7.4. DMPC, DMPG (racemic mixture), 1× crystallized and lyophilized HSA and horse skeletal muscle myoglobin (Mb) were purchased from Sigma Chemical Company. All solvents [chloroform, methanol, methyl ethyl ketone, dimethylformamide (DMF)] were obtained from Merck and were of spectroscopic grade. Stock solutions of MP were prepared in DMF and kept in the dark. Solutions were obtained by dilution with buffer and used without delay. For determination of the concentration of MP dissolved in DMF, a value of $\epsilon_{399} = 141{,}000\ M^{-1}\ cm^{-1}$ was determined by us, and used later.

Preparation of liposomes. The lipids were used as received. Small unilamellar vesicles (SUVs) were prepared as previously described (20). The phospholipid content of SUVs was quantified according to Rouser *et al.* (28).

Purification of HSA. In preliminary experiments it became evident that the HSA sample is not homogeneous as purchased; thus further purification was necessary. To obtain a homogeneous preparation of this protein, column chromatography was applied using a Pharmacia Superdex 75 column (2.6 × 50 cm) equilibrated with 50 mM phosphate buffer at pH 7.0. The molecular weight of HSA in the fractions was determined with the Pharmacia FPLC chromatography system (HR 10/30 column calibrated by Pharmacia molecular weight standard). Fractions of 67 kDa were lyophilized and stored at −20°C. The concentration of HSA was set using $\epsilon_{280} = 37{,}400\ M^{-1}\ cm^{-1}$ in phosphate buffer (29).

Preparation of apomyoglobin (ApoMb). Horse skeletal muscle Mb was purified by ion exchange column chromatography. The purity was checked and the isoelectric point was determined by isoelectric focusing (at p*I* 7.35). The native hemin was extracted from the protein by acid methyl ethyl ketone (30, 31). The apoprotein was dialyzed against phosphate buffer and used freshly. The concentration of ApoMb was determined using $\epsilon_{280} = 2 \times 10^4\ M^{-1}\ cm^{-1}$ in phosphate buffer (32).

Spectroscopy. Absorption spectra were recorded with a Cary 4E UV–Vis spectrophotometer. Fluorescence emission spectra were measured with an Edinburgh Instruments CD900 luminometer equipped with a Xe 75-W light source. Quartz cuvettes of 1-cm optical path were used and the emission was observed at 90° to the exciting beam. When the optical density was higher than 0.05, the correction for inner filter effect was calculated with the formula

$$I_{corr} = I_{obs} \times 10^{(OD_{ex}+OD_{em})/2}, \quad [1]$$

where I_{corr} and I_{obs} are the corrected and observed fluorescence intensities, and OD_{ex} and OD_{em} are the optical densities at the excitation and the emission wavelengths (33). The observed fluorescence intensities were also corrected for dilution. As in the measurements the signal/noise ratio was low; in some cases the slit widths were broad and the spectra were smoothed before evaluation.

Determination of equilibrium constants for MP–HSA ($K_{p,1}$) and MP–ApoMb ($K_{p,2}$) binding. To rule out the dimerization or aggregation of MP, a concentration range was determined where the fluorescence intensity depended on the concentration in a linear way. This range was limited toward the low concentration side also by the signal/noise properties of the experiment. We found that a MP con-

centration of 50 nM fulfills these requirements. MP concentration was kept constant and appropriate amounts of protein solution were added stepwise under stirring. For every step in the titration, a new MP solution was prepared just before the measurement. In the case of $K_{p,1}$ determination, the HSA/porphyrin molar ratio was always above 1.

The association constants were determined by a Scatchard representation (34, 35) that in our experiments corresponds to the formula

$$K_{p,i} \cdot (n[\mathrm{MP}]_{tot} - [\mathrm{protein}]_{compl}) = [\mathrm{protein}]_{compl}/[\mathrm{protein}]_{free}, \quad [2]$$

where $[\mathrm{MP}]_{tot}$ is the initial concentration of MP, $[\mathrm{protein}]_{free}$ and $[\mathrm{protein}]_{compl}$ are the concentrations of added and complexed protein, respectively, and n is the stoichiometry of the binding. According to Eq. [2], the fitted straight line intercepts the x and y axes, yielding n and $K_{p,i} \cdot n$, respectively (36). The concentration of free MP ($[\mathrm{MP}]_{free}$) in each solution was determined from the fluorescence intensity at 605 nm (excitation at 399 nm) and from the known initial MP concentration ($[\mathrm{MP}]_{tot}$). Under our experimental conditions, determination of $[\mathrm{protein}]_{compl}$ was not possible. Thus we approximated this value through the amount of MP molecules that were bound in the complex: $[\mathrm{protein}]_{compl} = [\mathrm{MP}]_{bound}$ supposing $n = 1$ (which is trivial for MP binding to ApoMb, but not in the case of HSA binding).

Determination of equilibrium constants for MP–DMPC liposome ($K_{L,1}$) and MP–DMPC/DMPG liposome ($K_{L,2}$) binding. The partition of MP between the lipid phase of vesicles and the bulk aqueous phase was studied similarly for both lipid compositions: a set of emission spectra were recorded while the lipid concentration was varied from 5×10^{-6} to 10^{-4} M and the concentration of MP was kept constant at 50 nM.

The association constants, $K_{L,i}$ ($i = 1, 2$), were calculated according to the formula

$$\frac{1}{I - I_0} = \frac{1}{(I_0 - I_{lip}) \cdot K_{L,i}} \cdot \frac{1}{[\mathrm{lipid}]} + \frac{1}{I_0 - I_{lip}}, \quad [3]$$

where the fluorescence intensities were determined at the wavelength of peak emission of MP bound to liposomes (625 nm at excitation of 399 nm); I, I_0, and I_{lip} are emission intensities in the presence of liposomes, in the absence of liposomes, and in the case of full incorporation, respectively (37). This formula takes into account the possible overlap of emission bands of free and bound MP molecules.

Observation of MP distribution between liposomes and protein (HSA, ApoMb). Liposomes in a molar ratio corresponding to saturation were added to MP dissolved in buffer. To complete the binding, the sample was kept at 32°C and stirred for 10 min. Then, increasing amounts of protein were added. The emission spectra of MP excited at 399 nm were recorded while varying the concentration of the protein.

Dynamic light scattering measurements. These measurements were performed with a commercially available spectrometer consisting of a BI-200SM goniometer and a BI-9000AT correlator. An Ar-ion laser (Omnichrome 543AP) operating at 488 nm was used as light source. The autocorrelation functions were recorded in real-time mode using a logarithmic time scale ranging from 1 to 100,000 μs.

The time autocorrelation function of the scattered intensity $g_2(\tau)$ was measured by the homodyne method and was converted to the scattered electric field autocorrelation function $g_1(\tau)$,

$$g_1(\tau) = \{[g_2(\tau) - \mathrm{BL}]/\mathrm{BL}\}^{1/2}, \quad [4]$$

where BL is the experimentally determined baseline. The spectra of the relaxation time (particle size distributions) were determined from $g_2(\tau)$ using the maximum entropy method (MEM) (38). The arithmetic mean of the data acquired in parallel experiments performed on the same sample was calculated and used for assessing particle size.

Microcalorimetry. Microcalorimetry was performed with a VP-DSC high-sensitivity differential scanning microcalorimeter (Microcal Inc.). The lipid concentration was 1 mM in each experiment. DSC curves were recorded in the absence and in the presence of HSA. (Control measurements were performed on the protein sample in the temperature range where the phase transition of the liposomes is observable.) As a reference solution, buffer or protein solution was used, respectively. The liposomes were incubated with HSA at room temperature for 1 h before the DSC measurements. After the sample was cooled to ~2°C and equilibrated, the heat capacity was measured between П6 and 40°C at a heating rate of 1°C/min. As the size-sensitive shape of the phase transition curve of SUVs (39) changes on reheating, the results of the first heating scans were compared. Since the phase transition curves consist of two maxima, the main transition temperature (T_m) is defined as the temperature at which the heat capacity reaches a local maximum. The first and second T_m (corresponding to increasing temperature) of each sample were reproducible within ±0.2 and ±0.1°C, respectively.

The deconvolution of phase transition curves was made according to the "independent non-two state" model using Origin 4.1 for DSC software package provided by Microcal. In the model a system composed of a number of structural domains A, B, . . . , is assumed. All of them are involved independently in a transition between A and A', B and B', ... Using the definition of van't Hoff enthalpy change (ΔH^*_A) from elementary thermodynamics, and from the assumptions that the transition is not of two states and it occurs without a change in total molar heat capacity of the system (C_p), the relationship of the temperature-dependent parameters can be given by

$$C_p(T) = \frac{K_A(T)\Delta H^*_{mA}\Delta H_{mA}}{(1 + K_A(T))^2 R T^2} + \ldots, \quad [5]$$

where ΔH_{mA} is the actual (i.e., calorimetric) molar enthalpy change, $K_A(T)$ is the temperature-dependent equilibrium constant for the transition that is calculated by

$$K_A(T) = \exp\left\{\frac{-\Delta H^*_{mA}}{RT}\left(1 - \frac{T}{T_{mA}}\right)\right\}, \quad [6]$$

where T_{mA} is the main transition temperature.

Before curve fitting, the baseline approximated by cubic spline was subtracted from the experimental data to remove ΔC_p effects if present (excess transition heat capacity).

RESULTS

1. MP–HSA and MP–Liposome Association

A detailed description of MP transfer from liposome to proteins requires the measurement of association constants, $K_{p,i}$ and $K_{L,i}$ prior to the distribution experiments.

1.1. MP–HSA association constant ($K_{p,1}$). The change in MP emission spectrum on fluorometric titration with HSA is shown in Fig. 1A (thick solid line in the absence of HSA, dotted and thin solid lines with increasing amount of HSA respectively). The addition of HSA to MP resulted in the appearance of a red-shifted MP fluorescence maximum: the peak emission

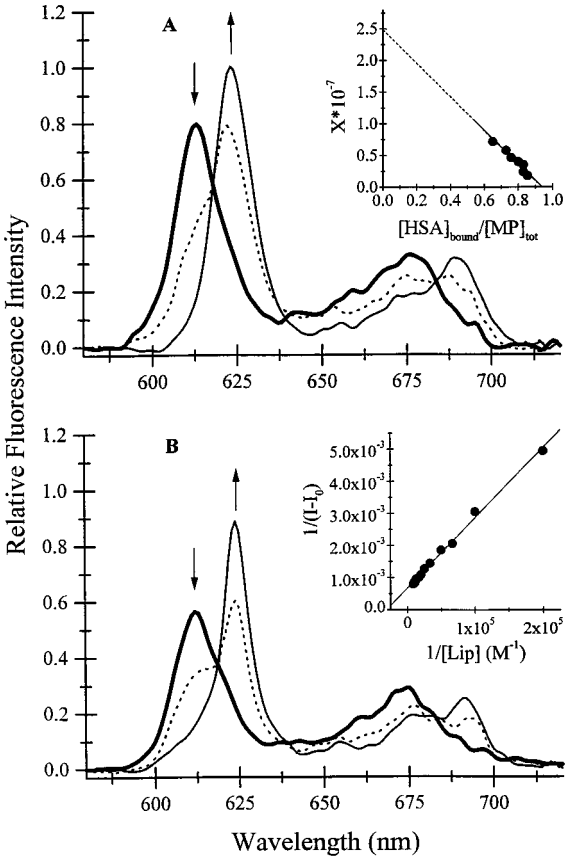

FIG. 1. (A) Change in MP emission spectrum (normalized to the saturation value) on binding to HSA at excitation of 399 nm (thick solid line in the absence of HSA, dotted and thin solid line with 9×10^{-8} and 1×10^{-6} M HSA, respectively). The arrows show the direction of the relative fluorescence intensity changes with increasing HSA concentration. Inset: Scatchard plot for determination of the MP–HSA association constant, $K_{p,1}$. The scale of the y axis, $X = ([HSA]_{bound}/[MP]_{tot})/[HSA]_{free}$ $(1/M)$. The plot leads to $K_{p,1} = (2.5 \pm 0.7) \times 10^7$ M^{-1}. (B) Change in MP emission spectrum (normalized) on binding to DMPC/DMPG liposomes at excitation of 399 nm (thick solid line in the absence of liposomes, dotted and thin solid line with 1.5×10^{-5} and 8×10^{-5} M liposomes, respectively). The arrows show the direction of the relative fluorescence intensity changes with increasing lipid concentration. Inset: Determination of MP–liposome association constant, $K_{L,i}$. According to Eq. [6], the slope of the fitted straight line is proportional with $K_{L,i}$.

of free aqueous MP is at 614 nm and that of MP bound to HSA is at 623 nm, respectively. The Scatchard representation of the data (Eq. [2]) is seen in the inset to Fig. 1A. The fact that the data points could be well fitted with a straight line (the correlation coefficient is -0.94 ± 0.05) confirmed the expected 1:1 stoichiometry of the binding, and supported that the binding of MP took place in the monomeric state, and only one kind of (primary) binding site was involved. The plot led to $K_{p,1} = (2.5 \pm 0.7) \times 10^7$ M^{-1}.

1.2. MP–lipid association constant ($K_{L,1}$, $K_{L,2}$). The fluorescence emission of MP as a function of lipid concentration is shown in Fig. 1B in the case of DMPC/DMPG liposomes. Similarly to the results of MP–HSA association experiments and in agreement with the emission spectra of MP in organic solvents a red shift was observed. This tendency did not depend on the lipid composition of the liposomes (not shown).

A respective plot according to Eq. [3] is shown in the inset to Fig. 1B in the case of DMPC/DMPG liposomes. The K_L values were $(1.3 \pm 0.3) \times 10^5$ M^{-1} ($K_{L,1}$) and $(3.2 \pm 0.6) \times 10^4$ M^{-1} ($K_{L,2}$) for DMPC and DMPC/DMPG liposomes, respectively.

2. Partition of MP between HSA and Liposomes

The emission spectra of MP bound to DMPC/DMPG liposomes recorded while varying the concentration of HSA are shown in Fig. 2D. It is obvious that MP rebinds to HSA: the intensity at 625 nm decreases, and a virtual spectral shift indicates that a new spectral component with increasing intensity appears at the shorter wavelength side. The position of the latter peak (623 nm) corresponds to the MP spectrum when bound to HSA. Similar spectral changes were observed in the case of DMPC liposomes (not shown), indicating that the transfer of MP from the liposomes to the HSA molecules occurs independently of vesicle charge.

To study the extent of the observed transfer, the relative fluorescence intensities were plotted as a function of relative HSA concentration. The results for DMPC and DMPC/DMPG liposomes are shown in Figs. 2A and 2B, respectively. To interpret the partition, we first approximated the phenomenon by supposing a competition between the association with liposomes and HSA and assuming the lack of interaction between the protein and the liposomes. Such a model (in the present work called "independent binding" model) leads to the formula (19)

$$I/I_{lip} = \frac{K_{L,i}(1 - I_{prot}/I_{lip})}{K_{L,i} + K_{p,i}\dfrac{[protein]}{[lipid]}} + I_{prot}/I_{lip}. \qquad [7]$$

$K_{L,i}$ and $K_{p,i}$ $(i = 1, 2)$ are the equilibrium constants for binding of MP to liposomes and to protein; I, I_{prot}, and I_{lip} are the fluorescence intensities of MP in the actual step, when totally bound to the protein, and when fully incorporated into liposomes, respectively. According to Eq. [7], a theoretical curve could be obtained for both lipid compositions using the previously determined association constants, $K_{p,1}$ and $K_{L,i}$, and the saturation values I_{lip} and I_{HSA} (Figs. 2A and 2B, solid line). The fit is rather good in the case of DMPC liposomes, but the presence of the negatively charged DMPG molecules causes significant deviation from the model: at higher HSA/lipid ratios, the association of

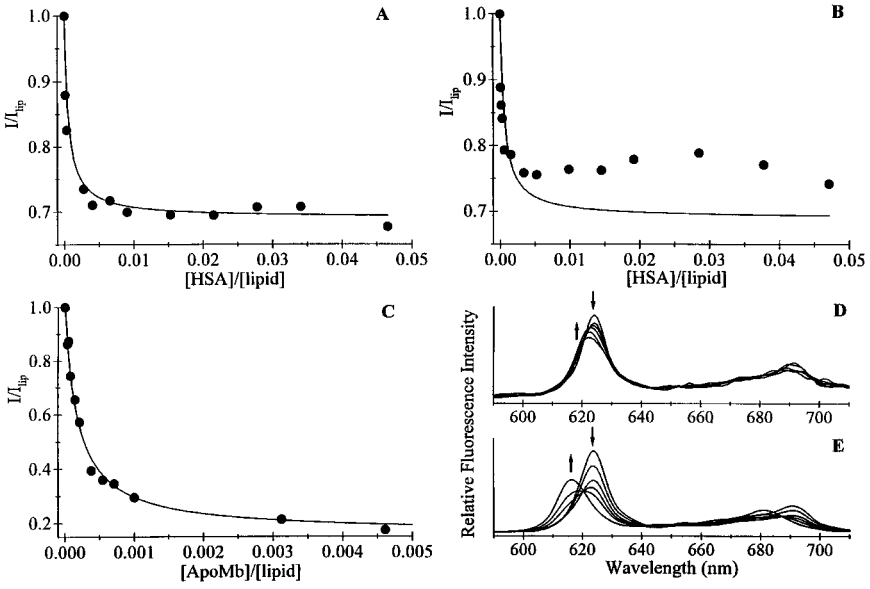

FIG. 2. Relative change in MP emission intensity at 625 nm on transferring from DMPC (A) or DMPC/DMPG (B) liposomes to HSA and from DMPC/DMPG liposomes to ApoMb (C) at excitation of 399 nm. The solid line is calculated according to the "independent binding" model (Eq. [7]). The model is invalid for the MP distribution between DMPC/DMPG liposomes and HSA. The change in MP emission spectrum on transferring from DMPC/DMPG liposomes to HSA (D) or to ApoMb (E). The arrows show the direction of the relative fluorescence intensity changes with increasing HSA or ApoMb concentration.

MP to HSA seems to be hindered. (The experimental data related to DMPC liposomes also has this kind of character, but the effect is much less pronounced.)

3. Partition of MP between apoMb and Liposomes

The partition experiment was repeated with ApoMb in the case of DMPC/DMPG liposomes to investigate if there is a specific interaction between the porphyrins and the liposomes that hinders the efflux of MP and to test the "independent binding" model (Eq. [7]). The spectral changes in this experiment are shown in Fig. 2E. As the difference between the maximum wavelengths emitted by the liposome- and ApoMb-bound MP (625 and 614 nm, respectively) is more significant compared with that obtained in the experiment with HSA, the partition effect is even more evident. The Scatchard plot (Eq. [2]) led to $K_{p,2} = (1.0 \pm 0.7) \times 10^8$ M^{-1} in this case. As shown in Fig. 2C, the experimental points fit well the theoretical curve corresponding to the independent partition model [the slope of the theoretical curve is different for HSA (Figs. 2A and 2C) because K_p is smaller). Thus, the possibility of a specific interaction between negatively charged liposomes and MP is ruled out.

4. Verification of Interaction between HSA and Liposomes in the Absence of Porphyrins

To elucidate liposome–HSA complex formation as a possible reason for the difference between the experimental results and the theoretical curve, discussed above (Fig. 2B), DSC experiments were performed. As the results were expected to be sensitive also for aggregation phenomena (39), dynamic light scattering data, evaluated by the MEM, were used to determine the particle size distribution functions of the samples before and after recording the phase transition. This type of analysis, however, has an inherent inaccuracy that strongly affects the distribution of particles with large radii. This is caused by the fact that while the signal-to-noise ratio of the data points in the autocorrelation function at longer correlation times becomes very low, the calculation is very sensitive to this part of the function that carries the information about the background of the curve as well. Thus, in the interpretation of the particle size distribution functions, the parameters (position and amplitude) concerning particles of larger size must be considered with caution. In the presentation of the light scattering results, we indicated the size range in the figures where the determination of the distribution function can be done with acceptable precision (see dashed vertical lines in the respective figures). Toward larger sizes, only tendencies could be concluded instead of absolute parameters.

4.1. Interaction between HSA and DMPC liposomes. The calorimetric curve of DMPC liposome solution in the absence of HSA is represented by the thick solid line in Fig. 3A. The curve consists of two phase transitions at 20.7 and 24.1°C. (Control measurements showed no phase transitions of the protein sample in

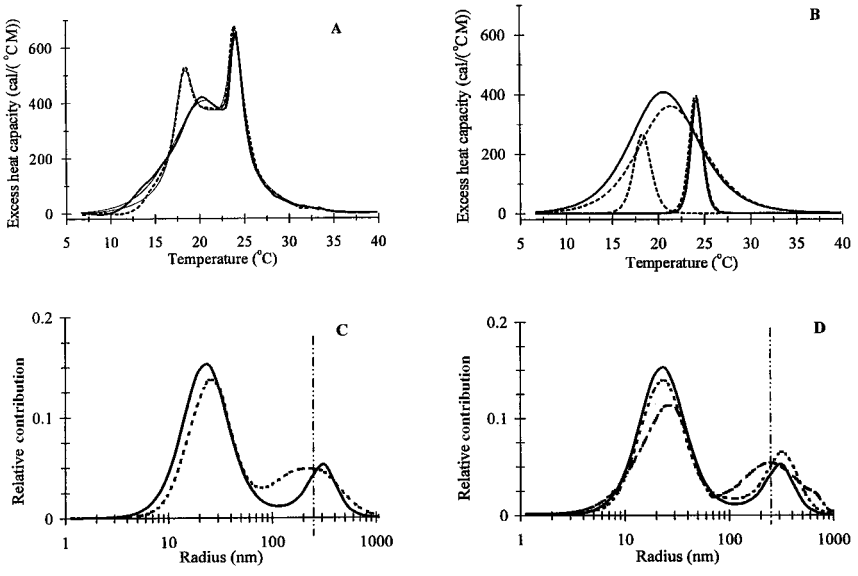

FIG. 3. (A) Phase transition of DMPC liposome in the absence (thick solid line) and in the presence (dashed line) of HSA. Thin solid lines represent the sum of fitted components. (B) Components resulting from the deconvolution of the phase transition curves of DMPC liposomes in the absence (solid line) and in the presence (dashed line) of HSA. (C) Particle size (radius) distribution functions of DMPC liposomes before (solid line) and after (dashed line) performing DSC. (D) Size distribution of DMPC liposomes in the absence of HSA (solid line) and in the presence of HSA before (dotted line) and after (dot–dashed line) the DSC experiment. The dashed vertical line indicates the size range where the size distribution function can be determined with acceptable precision (see Results).

the temperature range where the phase transition of the liposomes is observable.) The particle size (radius) distribution functions determined before and after performing DSC are shown in Fig. 3C by solid and by dashed lines, respectively. The light scattering results indicate two kinds of characteristic particle size and an increase in the relative number of larger particles during the DSC measurements. As the colloidal state of the liposome solution is changing during DSC measurement, the phase transition curve was deconvoluted using the "independent non-two-state" model approach (see Materials and Methods). An acceptable fit could be obtained by two components. These components are shown separately in Fig. 3B (solid lines) and their sum is compared with the experimental curve in Fig. 3A (thin solid line). Based on literature data (39) and the results of dynamic light scattering measurements (two populations of liposomes with different sizes), we identify the DSC component of lower melting temperature with the phase transition curve of SUVs (diameter $<$ 70 nm) and the second component of higher temperature with the phase transition curve of large unilamellar vesicles (LUVs), as discussed later. Addition of HSA significantly affected the DSC curve as shown in Fig. 3A by the dashed line. (The [HSA]/[lipid] concentration ratio was 0.01.) The deconvolution showed that the experimental curve cannot be fit with two components; three were needed. The components are shown in Fig. 3B by dashed lines, and their sum is overlaid on the original DSC curve in Fig. 3A. A new, narrower peak develops at a temperature (18.3°C) lower than that of the SUV population without HSA (20.7°C). The effect involves the liposomes of lower T_m values in the SUV population. The new component remains in the same melting range, and it has more cooperative phase transition. Based on an average enthalpy change for SUVs, it is possible to estimate the amount of SUV particles from the change in the respective peak area that was affected by HSA. It was 14 $\pm$ 2%. The phase transition of the LUV population is not affected. The new component was identified with SUV–HSA complexes.

The effect of HSA on the size distribution of liposomes is shown in Fig. 3D. Three distribution curves are presented corresponding to the conditions: liposome solution after an hour of incubation at room temperature (solid line); after identical incubation with HSA (dotted line); after the DSC experiment on a sample containing HSA (dot–dashed line). HSA causes the formation of larger particles even at room temperature, and the effect becomes more significant during the DSC measurement.

Control experiments were performed with liposomes of different average sizes by varying the intensity of sonication in the sample preparation procedure. The average radius size (calculated for the whole sample including SUVs and LUVs) could not be adjusted smaller than that analyzed above, but populations with larger average size could be obtained up to 450 nm as compared with 75 nm in the studied samples (both the SUV and LUV average sizes and their ratio

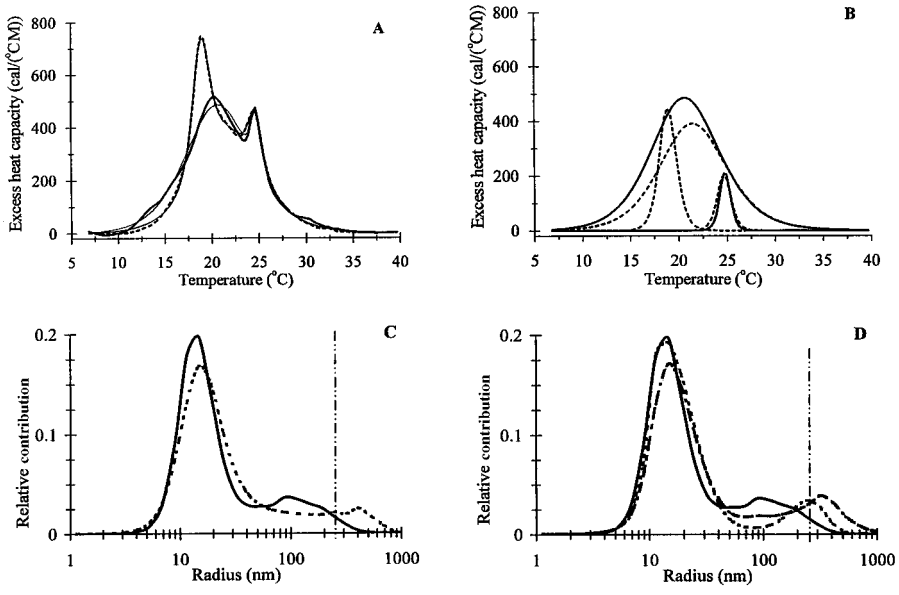

FIG. 4. (A) Phase transition of DMPC/DMPG liposomes in the absence (thick solid line) and in the presence (dashed line) of HSA. Thin solid lines represent the sum of fitted components in both cases. (B) Components resulting from the deconvolution of the phase transition curves of DMPC/DMPG liposomes in the absence (solid line) and in the presence (dashed line) of HSA. (C) Particle size (radius) distribution functions of DMPC/DMPG liposomes before (solid line) and after (dashed line) performing DSC. (D) Size distribution of DMPC/DMPG liposomes in the absence of HSA (solid line) and in the presence of HSA before (dotted line) and after (dot–dashed line) the DSC experiment. The dashed vertical line indicates the size range where the size distribution function can be determined with acceptable precision (see Results).

were different). The DSC curve was recorded before and after HSA addition in the case of these liposomes also. Their complex formation abilities were found to be similar (data not shown).

4.2. Interaction between HSA and DMPC/DMPG liposomes. The results for DMPC/DMPG liposomes are shown in Fig. 4 arranged similarly to Fig. 3. Comparison of Figs. 3 and 4 shows that the same experimental protocol leads to entirely different results depending on the lipid composition:

1. The size distribution function shows that the average size of DMPC/DMPG liposomes in both populations is smaller, and the amount of SUVs is significantly larger. This is in agreement with the disparity in the surface charge of the two lipid compositions: the repulsion between the negative surfaces promotes the formation of smaller liposomes (40). The average size after cooling also remains smaller.

2. In accordance with the size distribution difference, the contribution of the SUV population to the phase transition curve is much more significant in the case of DMPC/DMPG liposomes.

3. HSA addition affects both the DSC curve and the light scattering data similarly to the way it affects DMPC liposomes, but the appearance of a new, narrow transition peak within the original SUV transition peak at lower temperature is much more significant than in the previous case. The effect is estimated as involving 27 ± 2% of the SUV particles. The phase transition identified with the LUV population was not affected by HSA in this case either.

DISCUSSION

Binding of MP to HSA or Liposomes

In our experiments, $K_{p,1} = (2.5 \pm 0.7) \times 10^7\ M^{-1}$ was obtained for MP binding to HSA. This value fits the reported corresponding values for hematoporphyrin ($\sim 10^6\ M^{-1}$) and deuteroporphyrin ($\sim 5 \times 10^8\ M^{-1}$), respectively (41), and is in accordance with the concept that the binding strength increases with the hydrophobicity of the side chains. K_L values were $K_{L,1} = (1.3 \pm 0.3) \times 10^5\ M^{-1}$ and $K_{L,2} = (3.2 \pm 0.6) \times 10^4\ M^{-1}$ for DMPC and DMPC/DMPG liposomes, respectively, which are comparable to that found for deuteroporphyrin and DMPC sonicated liposomes $\sim 8 \times 10^4\ M^{-1}$ (19). The negatively charged DMPG molecules caused a decrease in the value of the association constant. Otherwise the spectrum on binding was always red shifted, independently of the lipid composition. This suggests that the porphyrin core becomes buried in the hydrophobic environment of the liposomes independently of the surface charge.

Validity of the "Independent Binding" Model for MP Distribution in Liposome/ApoMb and Liposome/HSA Systems

In the case of the DMPC/DMPG liposome/ApoMb system used as a control to test the validity of the

"independent binding" model (Eq. [7]), a good fit could be obtained using the independently determined K_p and K_L values. For liposome/HSA systems, the experimental points differed from the theoretical model depending on the surface charge of the liposomes. The strongest deviation was found for negatively charged liposomes in the range 0.01–0.04 HSA/lipid. In the case of DMPC liposomes, only a very slight difference was observed at somewhat higher ratios. From the comparison of these results we assumed the possibility of a direct interaction between HSA and the liposomes. For this, one has to rule out the difference in the binding of MP to ApoMb and to HSA as another possible reason for the observed difference in the transfer character. This can be achieved on the basis that (i) the same very low MP concentration was used for liposome/HSA systems as for liposome/ApoMb, where no MP dimerization occurs, so the existence of a dimer MP–HSA complex is ruled out (41). (ii) The difference between the model and the experimental points was found at higher HSA molar concentrations where the protein concentration was ~100 times higher than that of MP. In this way the binding of MP to other binding sites in HSA besides the primary porphyrin binding site (42) could be excluded. (iii) The competition between porphyrin and other candidates for binding to HSA in the case of MP partition may also be ruled out. It is well known that HSA can bind to a wide spectrum of molecules. There is evidence (43) that BSA is able to deplete the lipid components of the red blood cell membrane. Literature data (44), however, also show that liposomes can serve as lipid donors for the formation of albumin–lipid complexes only in the case of an overwhelming amount of albumin ([albumin]/[lipid] $>$ 100) and long incubation time (some hours). Thus, taking into account the experimental conditions in the present work, we could exclude the possibility of this type of interaction.

Based on these arguments we conclude that the deviation from the "independent binding" model in the case of HSA must be connected to the fact that the two binding partners of MP, HSA and the liposomes, are not independent of each other.

Evidence for HSA–Liposome Interaction from DSC and Dynamic Light Scattering

Earlier DSC experiments required a relatively high lipid concentration, so mainly multilamellar vesicles were examined. Today, the study of SUVs is also possible because of the significantly increased sensitivity of modern techniques. The phase transition phenomena of the two systems, however, are not identical. In the case of studying SUV particles, one has to consider for example that the experimental conditions of DSC measurements (cooling to low temperature, long experimental time) have a significant effect on the original structural features of the samples. As the thermograms of SUVs are relatively less widely known (compared with those of MLVs), we summarize below those most important characteristics that are available from the literature for DPPC and that we can use as a reference when evaluating our results (39, 45–47).

1. For SUVs, the transition temperature (T_m) critically depends on the vesicle size in the diameter range of about 35–70 nm. In this range T_m increases with increasing diameter. Above this range, the phase transition temperature becomes independent of size.
2. It was reported that on the initial cooling process included in the DSC experiment in the "heating mode," the gel-phase SUVs tended to fuse into LUVs.
3. The presence of SUVs in coexistence with LUVs results in a heat capacity curve with two phase transitions; the first one (maximum at lower temperature) corresponds to SUVs, the second one corresponds to LUVs.
4. The transition of SUVs takes place in a temperature range much broader than that observed for LUVs, since the curvature of the surface is more connected to structural order if the particles are small.

Both our DSC and dynamic light scattering results were in agreement with the enlisted concepts, and supported the identification of the two maxima seen in the phase transition curve of both liposome compositions (Fig. 3A, Fig. 4A, continuous lines). The change in DSC results on HSA addition unambiguously showed that HSA interacts with liposomes independently of their composition but to different extents. The mechanism was the same for both lipid compositions; HSA interacted with liposomes in the SUV population with lower T_m values but the LUV population was not changed. It is reasonable to suppose that some extent of structural distortion is a prerequisite in the reaction. In LUVs, this condition is missing and thus no interaction is observed. The phase transition of the SUV–HSA complex is of narrow temperature range, and the molar enthalpy change became somewhat higher with complex formation. (The area below the new component is somewhat higher than the missing area of SUVs.) These properties strengthen the view of a specific molecular complex formation that might even have a certain stoichiometry.

The uncertainty of the size distribution functions in the larger size range does not make it possible to derive a quantitative conclusion about the extent of the contribution of large particles. It seems evident, however, that HSA causes aggregation; the relative amount of larger particles increases. This effect, considered together with the fact that after HSA addition the peak of LUVs is not affected in the DSC curve, might mean that the larger particles are formed by the attachment

of small ones without fusion. In these aggregates of small liposomes HSA is thought to play a connecting role. These formations would melt at the temperature of SUVs, and the peak of LUVs would remain unaffected.

Role of Lipid Composition in the HSA–Liposome Interaction

Although the net charge of HSA is negative at pH 7.4, and the DMPC/DMPG liposomes are also negatively charged at this condition, complex formation was more effective in the case of DMPC/DMPG liposomes. Taking into account that the charged DMPG molecules have a strong tendency to form hydrogen bonds (48), and that the charge distribution on a protein surface is not homogeneous, we can conclude that both electrostatic interactions (repulsive and/or attractive) and hydrogen bond formation help to realize the right geometry required for HSA–liposome complex formation. The results show that a homogeneous, neutral surface does not represent such a good condition for formation of the suitable orientation required for the HSA binding. The decrease in T_m on complex formation, however, was similar for both lipid compositions. This indicates that HSA causes similar reorganization of the phospholipids in both types of liposomes. The packing of the lipid chains is less efficient in the complex, showing that complex formation involves partial penetration of the protein and deformation of the bilayer (49, 50). It is in agreement with the conclusions of earlier studies when interaction was found between albumin and liposomes (18, 51, 52).

Effect of HSA–Liposome Interaction on MP Distribution

The presence of HSA on the surface of liposomes hinders the transfer of MP from the liposomes to the protein. Under the condition when the surface is fully covered by HSA, efflux of MP would be inhibited by the HSA coating. Supposing that HSA interacts mainly with the surface of SUVs, we estimated the [HSA]/[lipid] concentration ratio when the HSA coat formation is complete. The average surface area of, e.g., liposomes 50 nm in diameter is about 8000 nm^2 supposing a globular shape. The approximate area of egg yolk lecithin phospholipid headgroups is 0.61 nm^2 for the inner surface and 0.74 nm^2 for outer surface (53). Thus the average lipid content corresponds to ~25,000 lipid molecules/liposomes supposing a unilamellar structure. The average surface area for one side of HSA approximated as a triangle from X-ray data is about 20 nm^2 (54). If all proteins would be bound to the surface of the liposomes, and this would mean a complete coating, the [HSA]/[lipid] concentration ratio would be 0.015. In the case of MP transfer from DMPC/DMPG liposomes to HSA, the strongest difference between the theoretical curve and the experimental points was found at somewhat higher [HSA]/[lipid] ratios (Fig. 2B). This may account for some of the albumin that remains unbound or for approximations in the estimation. The decline in fluorescence quantum yield at higher [HSA]/[lipid] ratios shows that there is another process that works against the inhibition effect of HSA and becomes dominant with increasing HSA. (It can be interpreted, for example, by an exchange of the bound protein molecules on the surface of liposomes). Since the probability of complex formation is smaller in the case of DMPC liposomes, the fully covered state would be realized at higher [HSA]/[lipid] ratios in this case. At high HSA concentration, however, the opposite process is more significant, so the system could not achieve the fully covered state even if the same model is applicable. This would explain the very slight inhibition effect of HSA binding in the case of DMPC liposomes (Fig. 2A).

CONCLUSIONS

The porphyrin carrier function of HSA is strongly perturbed by the presence of liposomes, since HSA interacts with their surface. This interaction, however, depends on the size and lipid composition of the vesicles: small, negatively charged liposomes are more favorable for the binding. As a result of the interaction, the lipid surface can be saturated by HSA. Under these saturating conditions, porphyrin transport becomes inhibited.

ACKNOWLEDGMENTS

The authors thank Professor F. Reig at the Department of Peptides, CID, CSIC, Barcelona, Spain, for valuable discussions concerning liposome–peptide interactions, and Dr. T. Gilányi and I. Varga at the Department of Colloid Chemistry of Eötvös L. University Budapest, Hungary, for help in the light scattering experiments. Support through TEMPUS JEP Program 2113/92 and Professors K. Medzihradszky and F. Hudecz is greatly appreciated. The professional help of Mrs. R. Markács and Mrs. É. Bányai in sample preparation is highly appreciated.

This work was supported by Hungarian Grants ETT 425/1996, FKFP 0166/97, 1191/97, and OTKA T 022370, 25545 and by DFG (J.F.).

REFERENCES

1. Bogorad, L. (1979) *in* The Porphyrins (Dolphin, D., Ed.), Vol. 5., pp. 125–172, Academic Press, New York.
2. Muller-Eberhard, U., and Morgan, W. T. (1975) *Ann. N. Y. Acad. Sci.* **244,** 624–650.
3. Ricchelli, F., Jori, G., Moreno, G., Vinzens, F., and Salet, C. (1990) *J. Photochem. Photobiol. B* **6,** 69–77.
4. Cannon, J. B., Kuo, F. S., Pasternack, R. F., Wong, N. M., and Müller-Eberhard, U. (1984) *Biochemistry* **23,** 3715–3721.
5. Moan, J. (1986) *Photochem. Photobiol.* **6,** 681–690.

6. Henderson, B. W., and Dougherty, T. J. (1992) *Photochem. Photobiol.* **55,** 145–157.
7. Dayan, F. E., Duke, S. O., Faibis, V., Jacobs, J. M., and Jacobs, N.J. (1998) *Arch. Biochem. Biophys.* **351,** 27–34.
8. Geze, M., Morliere, P., Maziere, J. C., Smith K. M., and Santus, R. (1993) *J. Photochem. Photobiol. B* **20,** 23–35.
9. Vever-Bizet, C., and Brault, D. (1993) *Biochim. Biophys. Acta* **1153,** 170–174.
10. Sinclair, P. R., and Granick, S. (1976) *Ann. Clin. Res.* **8,** 250–258.
11. Granick, S., and Beale, S. I. (1978) *Adv. Enzymol. Relat. Areas Mol. Biol.* **46,** 33–203.
12. Granick, S., Sinclair, P., Sassa, S., and Grieninger, G. (1975) *J. Biol. Chem.* **250,** 9215–9225.
13. Hoekstra, D., and Scherphof, G. (1979) *Biochim. Biophys. Acta* **551,** 109–121.
14. Cochran, F. R., Connor, J. R., Roddick, V. L., and Waite, B. M. (1985) *Biochem. Biophys. Res. Commun.* **130,** 800–806.
15. Devine, D. V., Wong, K., Serrano, K., Chonn, A., and Cullis, P. R. (1994) *Biochim. Biophys. Acta* **1191,** 43–51.
16. Reddi, E., and Jori, G. (1988) *Rev. Chem. Intermediates* **10,** 241–268.
17. Coleman, R. (1987) *Biochem. J.* **244,** 249–261.
18. Law, S. L., Lo, W. Y., and The, G. W. (1994) *Drug Dev. Ind. Pharm.* **20,** 1411–1423.
19. Kuzelová, K., and Broult, D. (1994) *Biochemistry* **33,** 9447–9459.
20. Bárdos-Nagy, I., Galántai, R., Kaposi, A. D., and Fidy, J. (1998) *Int. J. Pharm.* **175,** 255–267.
21. Margalit, R., Shaklai, N., and Cohen, S. (1983) *Biochem. J.* **209,** 547–552.
22. Szocs, K., Gabor, F., Csik, G., and Fidy, J. (1999) *J. Photochem. Photobiol B* **50,** 8–17.
23. Kagava, Y. (1974) *in* Methods in Membrane Biology (Korn, E. D., Ed.), Vol. 1., pp. 201–235, Plenum, New York.
24. Salet, C., and Moreno, G. (1990) *J. Photochem. Photobiol. B* **4,** 133–150.
25. Klein, S. D., Walt, H., and Richter, C. (1997) *Arch. Biochem. Biophys.* **348,** 313–319.
26. Wohlgemuth, R., Waespe-Sarcevic, N., and Seelig, J. (1980) *Biochemistry* **19,** 3315–3321.
27. Durvasula, R. V., and Huang, C.-h. (1999) *Biochim. Biophys Acta* **1417,** 111–121.
28. Rouser, G., Fleisner, S., and Yamamoto, A. (1970) *Lipids* **5,** 494–496.
29. Reddi, E., Lambert, C. R., Jori, G., and Rogers, M. A. (1987) *Photochem. Photobiol.* **45,** 345–351.
30. Teale, F. W. J. (1959) *Biochim. Biophys. Acta* **35,** 543.
31. Kaposi, A. D., Fidy, J., Stavrov, S. S., and Vanderkooi, J. M. (1993) *J. Phys. Chem.* **97,** 6319–6327.
32. Morishima, I., Ogawa, S., Inubushi, T., Yonezawa, T., and Iizuka, T. (1977) *Biochemistry* **16,** 5109–5115.
33. Lakowitz, J. R. (1983) Principles of Fluorescence Spectroscopy, pp. 44, 303–309, Plenum, New York.
34. Scatchard, G. (1949) *Ann. N. Y. Acad. Sci.* **51,** 660–672.
35. Reddi, E., Rodgers, M. A. J., Spikes, J. D., and Jori, G. (1984) *Photochem. Photobiol.* **40,** 415–421.
36. Schwarz, G. (1976) *Biophys. Struct. Mechanism* **2,** 1–12.
37. Brault, D., Vever-Bizet, C., and Doan, T. L. (1986) *Biochim. Biophys. Acta* **857,** 238–250.
38. Bryan, R. K. (1990) *in* Maximum Entropy and Bayesian Methods, (Fougere, P. F., Ed.), pp. 221–232, Kluwer Academic, Dordrecht/Norwell, MA.
39. Biltonen, R. L., and Lichtenberg, D. (1993) *Chem. Phys. Lipids* **64,** 129–142.
40. Grit, M., and Crommelin, D. J. A. (1993) *Chem. Phys. Lipids* **64,** 3–18.
41. Rotenberg, M., and Margalit, R. (1985) *Biochem. J.* **229,** 197–203.
42. Moehring, G. A., Chu, A. H., Kurlansik, L., and Williams, T. J. (1983) *Biochemistry* **22,** 3381–3386.
43. Connor, J., Pak, C. H., Zwaal, R. F. A., and Schroit, A. J. (1992) *J. Biol. Chem.* **267,** 19412–19417.
44. Zborowski, J., Roerding, F., and Scherphof, G. (1977) *Biochim. Biophys. Acta* **497,** 183–191.
45. Suurkuusk, J., Lentz, B. R., Barenholz, Y., Biltonen, R. L., and Thompson, T. E. (1976) *Biochemistry* **15,** 1393–1401.
46. Lichtenberg, D., Freire, E., Schmidt, C. F., Barenholz, Y., Felgner, P. L., and Thompson, T. E. (1981) *Biochemistry* **20,** 3462–3467.
47. Barrow, D. A., and Lentz, B. R. (1980) *Biochim. Biophys. Acta* **597,** 92–99.
48. Durvasula, R. V., and Huang, C.-h. (1999) *Biochim. Biophys. Acta* **1417,** 101–110.
49. Chapman, D., and Urbina, J. (1974) *J. Biol. Chem.* **249,** 2512–2521.
50. Papahadjopoulos, D., Moscarello, M., Eylar, E. H., and Isac, T. (1975) *Biochim. Biophys. Acta* **401,** 317–335.
51. Lis, L. J., Kauffman, J. W., and Shriver, D. F. (1976) *Biochim. Biophys. Acta* **436,** 513–522.
52. Hoekstra, D., and Scherphof, G. (1979) *Biochim. Biophys. Acta* **551,** 109–121.
53. Huang, C., and Mason, J. T. (1978) *Proc. Natl. Acad. Sci. USA* **75,** 308–310.
54. He, X. M., and Carter, D. C. (1992) *Nature* **358,** 209–215.